Materials Chemistry and Physics 282 (2022) 125934

Contents lists available at ScienceDirect

Materials Chemistry and Physics

journal homepage: www.elsevier.com/locate/matchemphys

Fabrication of selective gas sensors using Fe_3O_4 nanoparticles decorated with CuO

Ahmad I. Ayesh *, Belal Salah

Physics Program, Math., Stat. and Physics Department, College of Arts and Sciences, Qatar University, Doha, Qatar

HIGHLIGHTS

- H_2S gas sensors were produced based on nanoparticles of Fe_3O_4 decorated with CuO.
- The nanoparticles were synthesized by a coprecipitation method.
- The sensors were sensitive at room temperature for H_2S concentration of 1.0 ppm.
- The minimum response times was 1.0 min.
- The sensors were stable for multiple application cycles.

ARTICLE INFO

Keywords:
Decorated nanoparticles
Metal-oxide
Gas sensor
Fe_3O_4
CuO
H_2
H_2S

ABSTRACT

Metal-oxide nanoparticles are regarded as favorable candidates for different device applications including gas sensors. Decoration of nanoparticles with smaller ones of different types enables taking advantage of the physical and chemical characteristics of both core and decorate nanoparticles. Fe_3O_4 nanoparticles decorated with CuO are produced in this work by a coprecipitation method and investigated for their application for H_2S gas sensor devices. The average size of Fe_3O_4 nanoparticles is 33.33 ∓ 5.55 *nm* while the average grain size of the CuO nanoparticles is 9.72 ∓ 1.39 *nm*. Gas sensors are fabricated by depositing dispersed nanoparticles on substrates with pre-printed interdigitated electrodes. Impedance spectroscopy is utilized to investigate the electrical characteristics of fabricated devices, where their activation energy is evaluated to 0.386 ± 0.076 *eV*. The fabricated sensors are found to be selective to H_2S and sensitive to low concentrations, as low as 1.0 ppm, with minimum response time of 1.0 min. The produced sensors indicate potential for field applications due to their various features that include simplified and practical fabrication procedure, low power needs, high sensitivity, reasonable response time, and magnetic properties of nanoparticles that facilitate their recycling.

1. Introduction

Maintaining high quality of air that is suitable for a healthy life style is becoming a serious issue considering the increase of industrial activities that extract further hazard gases [1]. Among those gases, hydrogen sulfide (H_2S) that is produced by human activities such as crude oil extraction, petroleum refining activities, mining of natural coal, and extraction of sewage water. It is also produced from natural resources that include bacterial disintegration of plant and animal waste, slack water with low concentration of oxygen, volcanoes, mineral springs, and others [2]. Highly sensitive H_2S sensors are essential for monitoring and control of environmental quality, since H_2S presence with concentrations of tens of ppm might threaten human life [3]. Conductometric gas sensors represent reliable category of sensors with many practical applications since they are portable, have low production cost, small in size, and present direct reading [4,5]. The recent developments in producing custom-designed nanomaterials vastly enhanced the features of the produced gas sensors, thanks to their high number of reactive sites generated by their high surface area as compared with their volume [6,7].

Nanoparticles of metal-oxides are known for their semiconductor properties and they are implemented in various device applications [8,9]. For example, they are utilized for hazardous gas sensors due to their effective production with novel features at a practical cost [10,11].

* Corresponding author. Qatar University, Doha, Qatar.
E-mail address: ayesh@qu.edu.qa (A.I. Ayesh).

https://doi.org/10.1016/j.matchemphys.2022.125934
Received 6 July 2021; Received in revised form 8 January 2022; Accepted 26 February 2022
Available online 10 March 2022
0254-0584/

Intrinsic copper oxide of cupric-oxide form (CuO) is known as an p-type semiconductor with a band gap in the range 1.21–1.51 eV [12,13]. It is also known for its high affinity towards adsorption of H_2S gas at low temperature [14]. On the other hand, iron oxide (Fe_3O_4) exhibits a magnetic crystal with metal deficient at octahedral sites, and could have either n-type or p-type semiconducting properties according to the degree of its metallic polarization [15]. Both metal-oxides are known for their reasonable synthesis cost, high stability, and environmental suitability [16]. Decoration of Fe_3O_4 with CuO nanoparticles introduces new opportunities for producing a new class of novel H_2S sensors [17,18] that are functional at low temperatures and exhibit magnetic features that permit manipulating their location and retrieving them after utilization for recycling.

We report on the synthesis of Fe_3O_4 nanoparticles decorated with CuO and their utilization for H_2S sensor applications. Herein, Fe_3O_4 nanoparticles are synthesized first and then CuO nanoparticles are deposited on their surfaces. The nanoparticles are synthesized by a coprecipitation method and deposited on substrates with pre-printed interdigitated electrodes to produce the devices. The incorporation of Fe_3O_4 nanoparticles with CuO allows utilization of the magnetite feature of Fe_3O_4 for controlling their location and recycling while taking advantage of the high affinity of CuO nanoparticles towards H_2S for its sensing. The morphology of nanoparticles is tested by scanning and transmission electron microscopy, while electrical properties are explored by impedance spectroscopy technique. The response of the devices toward H_2S and H_2 gases is inspected as a function of gas concentration and temperature. The produced sensor devices are discriminatory to H_2S and sensitive to low concentrations, as low as 1.0 ppm, with minimum response time of 1.0 min.

2. Experimental

2.1. Materials

$FeCl_3.6H_2O$ (99%), $FeCl_2{\cdot}4H_2O$ (99%), $CuNO_3$ (99.99%), (3-aminopropyl)trimethoxysilane (APTMS) 97%, and sodium hydroxide (98%) were all purchased from Sigma-Aldrich. Anhydrous isopropanol, NH_4OH (25%), and trisodium citrate were acquired from BDH.

2.2. Synthesis of Fe_3O_4 nanoparticles decorated with CuO

This first step was to produce the Fe_3O_4 nanoparticles. Those nanoparticles were synthesized by a coprecipitation method [19], by 2:1 M solution of Fe^{3+} and Fe^{2+}, and 1 wt% of trisodium citrate as a surfactant followed by reduction using NaOH. Herein, NaOH was used as a reducing agent under vigorous stirring until the pH reached to about 10, then kept for 20 min under stirring. The black precipitate was washed several times with deionized water and alcohol to remove any reactants and impurities. Finally, the precipitate was dried at 80 °C for 10 h.

To decorate the Fe_3O_4 nanoparticles with CuO, the Fe_3O_4 surfaces were functionalized by amino groups using APTMS in isopropanol to get uniform decoration and increase the disparity after the annealing step. Herein, 1 wt% of Fe_3O_4 nanoparticles dispersed in isopropanol was sonicated for 20 min 200 μL APTMS was added and refluxed at 80 °C overnight. The precipitate was washed with ethanol and dispersed in 0.25 gm of $CuNO_3$ isopropanol solution and stirred for 15 min. Under vigorous stirring, NH_4OH was added gradually. The precipitate was washed with deionized water and alcohol and dried at 80 °C. Nanoparticles were then annealed at 450 °C for 2 h, where the temperature was increased at a rate of 5 °C/min. This annealing enhanced their crystal quality as observed by x-ray diffraction tests below.

2.3. Sensor fabrication

To fabricate a gas sensor, small amount of the produced nanoparticles' powder was dispersed in ethanol, and placed on a sonicator until dispersed. Few drops of the dispersed solution were deposited on a printed substrate that contained interdigitated gold electrodes with electrode separation of: 100 μm for H_2S response tests, and of 10μm for H_2 response tests. The 10 μm electrode separation was used for H_2 sensors since it is suitable for the low sensitivity of nanoparticles toward H_2 gas, while the 100 μm electrode separation was found to be suitable to be used to detect low and high H_2S concentrations at room temperature (25 °C) due to the highly sensitivity of nanoparticles toward H_2S. It should be noted that devices with different contact areas exhibit different resistances, but the response measurements are based on relative change of resistance. Each device was then dried inside a gas chamber with dry flow of nitrogen of 30 sccm for 20 min to clean the ambient from any impurities and moister. Electrical wires were connected to the interdigitated electrodes by silver paste. Each fabricated sensor was placed on top of a ceramic heater fixed inside a Teflon chamber for the purpose of gas sensing measurements. A thermocouple of K-type was inserted on top of the sensor to quantify its temperature and enable temperature control. Pictures of the Teflon chamber and the device can be found in references. It should be noted that other gases can be tested using the fabricated devices, however, only H_2S and H_2 gases are tested due to the focus of the current work and their availability in our lab.

2.4. Characterization

A scanning electron microscope (SEM) model NanoSEM-450 of Nova made that contains an energy dispersive x-ray spectroscopy (EDS) system was engaged to investigate the morphology and chemical composition of Fe_3O_4 and CuO nanoparticles. A high resolution transmission electron microscope (TEM) of FEI made (model Tecnai TF20 G2) was used to determine the nanoparticle size and verify the decoration of nanoparticles (CuO on Fe_3O_4). Nanoparticle sizes were calculated using ImageJ software. It should be noted that the lattice fringes could not be resolved due to the magnetic effect of the nanoparticles. An EDS system for elemental mapping attached to the TEM was also used to further confirm the composition of nanoparticles. Molybdenum grids were used for TEM imaging along with the associated elemental mapping by EDS.

The composition of the synthesized Fe_3O_4/CuO nanoparticles was further investigated by x-ray diffraction (XRD) by employing an Empyrean XRD system. XRD characterization was also used to identify the structure of the synthesized nanoparticles. The XRD measurements were performed by taking advantage of Cu-K_α emission peak with a characteristic wavelength of $\lambda = 1.5405$ Å. During XRD tests, the measurements were scanned through the angle range of $2\theta = 20.0 - 80.0^\circ$ within a step size of 0.02°.

Electrical impedance ($Z(\omega)$) characterization was established using an impedance–gain–phase meter of Solarton made (model 1260A). All impedance measurements were performed at controlled temperatures inside the Teflon chamber. The samples were measured using a two points scheme for a granular film of nanoparticles between two gold electrodes. The electrical impedance was measured at variable frequencies ($\omega = 2\pi f$, f is the frequency and it was ranged between 1 - 10^6 Hz) and resolved into real ($Z'(\omega)$) and imaginary ($Z''(\omega)$) elements. Therefore, the impedance could be expressed in terms of a complex equation as $Z(\omega) = Z'(\omega) - iZ''(\omega)$ with i is the complex number. The variation of $Z''(\omega)$ as a function of $Z'(\omega)$ was demonstrated by a Nyquist plot that involves the frequency as an implicit variable. A Scribner made software (Zview) was employed to control the impedance measurements, produce Nyquist plots, and fit the dependence of $Z''(\omega)$ on $Z'(\omega)$ to predict the equivalent circuit of the nanoparticle films.

Gas response tests were performed by employing mass flow meters from Bronkhorst company. Herein, the target gas (H_2S or H_2) was mixed with zero air (without hydrocarbons) at particular ratios [20]. The gas/air flow rate was measured by sccm, thus, the concentration of a gas relative to air was identified in ppm by dividing its flow rate to that of air

multiplied by million. The diluted gas was then injected into the gas test Teflon chamber while sealed with continuous flow. The test chamber guarantee that the gas response tests are performed at controlled humidity. The target gases were selected based on the national interest and the availability in our lab. The gas response was measured by a source measurement unit (SMU) (Keithley Instruments - model 238) within a temperature range of 25–90 °C. A fixed bias of 15.0 V was applied crosswise the sensor electrodes while electrical current variation was observed. The sensor response was denoted as $|\frac{R_{gas}-R_{air}}{R_{air}}|$, with R_{gas} and R_{air} were electrical resistance values of a sensor with the existence of the target gas and the reference air, respectively. Current-voltage (I(V)) characterization were performed before and after gas sensing cycle for each sensor.

3. Results and discussion

Nanoparticles of Fe_3O_4 decorated with CuO are synthesized by coprecipitation procedure. The morphology of the produced Fe_3O_4 nanoparticles is depicted in Fig. 1(a). Their composition is by EDS analysis in Fig. 1(b). Furthermore, the morphology of the synthesized Fe_3O_4 nanoparticles decorated by CuO is shown in Fig. 1(c). Fig. 1(a)–(c) reveal individual nanoparticles of semicircular shapes as well as their agglomerates. The addition of APTMS decrease the agglomeration as shown by the SEM image, while the mild agglomeration of the nanoparticles may be referred to the magnetic nature of the Fe_3O_4 particles. The composition of the produced nanoparticles is confirmed by EDS measurements as demonstrated in Fig. 1(d). The EDS elemental mapping (inset of Fig. 1(c)) further confirms the composition of the synthesized nanoparticles. The uniform elemental distribution is an indication of the uniform decoration and homogeneity distribution. TEM images in Fig. 1 (e) – 1(f) reveal agglomerates of nanoparticles. The figures show large nanoparticles of Fe_3O_4 decorated with smaller nanoparticles of CuO (the circles in Fig. 1(f) that highlight an example of the decoration). The average grain size of Fe_3O_4 nanoparticles is $33.33 \mp 5.55\ nm$ while the average size of the CuO nanoparticles is $9.72 \mp 1.39\ nm$. The error of both sizes is taken as the stander deviation of the distribution.

The composition of the CuO/Fe_3O_4 nanoparticles and their crystal structures are further investigated by XRD analysis. Fig. 2 illustrates the

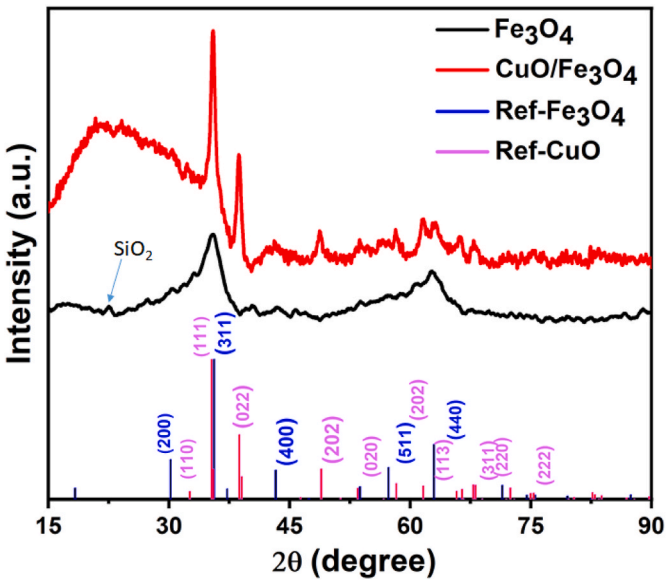

Fig. 2. *XRD spectra of both* Fe_3O_4 *and* CuO/Fe_3O_4 *nanoparticles together with Miller indices and reference patterns* ICSD:250,540 for Fe_3O_4 and ICSD:67,850 for CuO17.

XRD spectra of as prepared Fe_3O_4 and decorated CuO/Fe_3O_4 nanoparticles as well as the reference patterns of Fe_3O_4 and CuO. The XRD spectrum of Fe_3O_4 nanoparticles exhibits a low strength that is due to the poor crystallinity of Fe_3O_4 which are related to the used preparation method. Therefore, the observed broadening of the XRD peaks could be misleading if utilized to calculate the nanoparticle size. This synthesis procedure of nanoparticles involves the functionalization with Fe_3O_4 amino groups using APTMS and the formation of SiO_2 on their outer layer as revealed by the SiO_2 peak in Fig. 2. The XRD spectrum of CuO/Fe_3O_4 nanoparticles on the other hand exhibits higher strength due to the dilution of Fe_3O_4 nanoparticles by the crystalline CuO as well as the effect of annealing process which increase the crystallinity degree of Fe_3O_4 without changing the other phases. The figure also reveals the

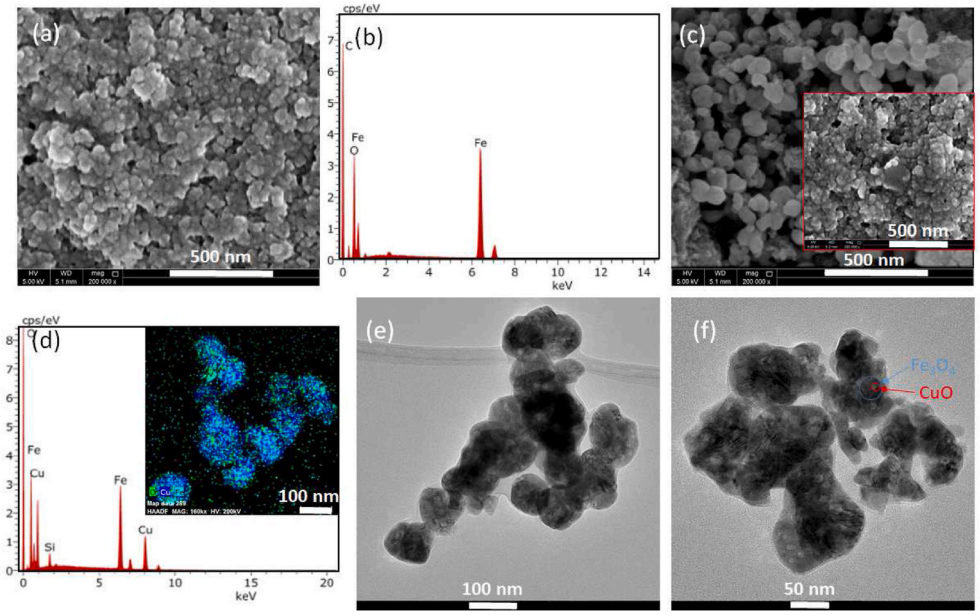

Fig. 1. *(a) SEM image of the synthesized* Fe_3O_4 nanoparticles. *(b) EDS analysis of* Fe_3O_4 *nanoparticles. (c) SEM image of the synthesized* CuO/Fe_3O_4 nanoparticles. *(d) EDS along with elemental composition analysis of* CuO/Fe_3O_4 *nanoparticles. (e) and (f) TEM images at different magnifications of synthesized* CuO/Fe_3O_4 nanoparticles. *The circles in (f) show examples of* Fe_3O_4 *and CuO nanoparticles.*

referral patterns of Miller indices for the individual Fe_3O_4 nanoparticles (ICSD:250,540, ICDD:98-025-0540) [21] and CuO nanoparticles (ICSD:67,850, ICDD:98-006-7850) [22]. The Fe_3O_4 nanoparticles exhibit cubic crystal structure, while CuO nanoparticles exhibit monoclinic crystal structure. The good matching between the XRD spectrum of CuO/Fe_3O_4 and the individual references of CuO and Fe_3O_4 indicates that each type of nanoparticles maintain its integrity during the decoration.

Electrical characterizations are investigated for CuO/Fe_3O_4 nanoparticles at different temperatures by means of impedance measurements under a continuous flow of zero air inward the test chamber to eliminate the effect of ambient moisture. The tests are performed for samples of the parallel plate capacitor structure by scanning ω and measuring both $Z''(\omega)$ and $Z'(\omega)$. Fig. 3(a) shows the Nyquist plots of CuO/Fe_3O_4 nanoparticles at different temperatures. The figure illustrates that the dependence of $Z''(\omega)$ on $Z'(\omega)$ can be represented by a single semicircle at each temperature. The unique semicircles illustrate that each CuO/Fe_3O_4 nanoparticles' film may be represented by an equivalent of a single pair of resistive and capacitive components that are connected into parallel [23]. It should be noted her that the single semicircle is also an indication of excellent interface between the electrodes and the CuO/Fe_3O_4 nanoparticles' film with low resistance (since a second semicircle does not appear). The semicircle is allocated to the kinetic process of charge transmission that increases with frequency, rather than ions' transmission (current generated at low temperatures is mainly electronic) that have large relaxation time thus their transmission is trivial. Within the kinetic process, grain boundaries govern the value of resistance while depletion regions of CuO/Fe_3O_4 nanoparticle film govern the value of the capacitance [23]. The figure also reveals that the semicircle radius (that represents the dc resistance of the CuO/Fe_3O_4 nanoparticles) decreases with rising the temperature which indicates a negative temperature coefficient of the resistance [24]. Such a negative temperature coefficient of the resistance is due to the increase in electron transfer rate between the valence and conduction bands that causes an increase in carrier concentration because of high energy at elevated temperatures. As the temperature increases, charge carriers attain energy essential for their transfer and diffusion to the metal electrodes, that are driven by electric force generated from the voltage difference.

The semicircles in Nyquist plots are fitted using Zview to identify the dc resistance (R) as well as capacitance of CuO/Fe_3O_4 nanoparticles' films. The resistance is then utilized to identify the resistivity (ρ) according to $\rho = \frac{Rl}{A}$, where A and l represent the cross sectional area and length of current path of the CuO/Fe_3O_4 nanoparticles' films, respectively. The temperature dependence ($\frac{1000}{T}$) of electrical resistivity (on logarithmic scale) is demonstrated in Fig. 3(b). The figure illustrates the observation of negative temperature coefficient of resistivity detected in Fig. 3(a), which is normally expected for granular and nanoparticles systems of metal-oxides [25]. The activation energy (E_a) is determined from Fig. 3(b) using an Arrhenius equation: $\rho = \rho_0 e^{\frac{E_a}{k_B T}}$, with k_B and ρ_0 denote Boltzmann constant and temperature independent constant, respectively. Therefore, the temperature dependence of the resistivity is fitted into linear equation that yields an activation energy of $0.386 \pm 0.076\ eV$. This value of E_a is rational when compared with analogous systems of nanoparticles' films of metal-oxides [14]. Furthermore, this value of E_a depends on different factors such as chemisorbed oxygen and ionized native defects, and it is higher for metal-oxides nanoparticles than that of conducting (metal) nanoparticles since the carrier concentration is lower for metal-oxides [24].

The produced nanoparticles' films are tested for their gas response as conductometric sensors. It should be noted that the pristine Fe_3O_4 nanoparticles are not sensitive to either of H_2S or H_2, while it is not possible to measure the sensitivity of the individual CuO nanoparticles since they were synthesized in-situ on top of Fe_3O_4. The sensor gas response towards H_2 gas as a function of temperature of a produced CuO/Fe_3O_4 nanoparticles' based sensor is presented in Fig. 4. The injection of air and response measurements are continuous as well as simultaneous, and the response signals appear when the target gas is injected. The figure reveals that the sensor response is minimal during exposure to the reference air, and it increases upon exposure to H_2. The sensor response proportional with H_2 continent and it is higher at 90 °C as compared with that at 25 °C. Nevertheless, the figure demonstrates that the sensor can detect concentrations of the order of kilo ppms. It should be noted that the SiO_2 is not expected to contribute to the sensing mechanism as it is known of its low affinity (compared with CuO) towards both H_2 and H_2S. Fig. 5(a) and (b) demonstrate the sensor gas response towards H_2S gas at different temperatures of the produced CuO/Fe_3O_4 based sensors. The sensor response increases with temperature, although it is functional at 25 °C which is considered an important advantage of the present sensor. Furthermore, the other operation temperatures of the sensor are still low temperatures (maximum of 90 °C). The maximum response of the sensor towards H_2S gas is at 55 °C. The sensor response signal returns back to reference once H_2S gas flow is stopped and the chamber is "washed" by air. The figure reveal that the sensor is more sensitive towards H_2S gas (as compared with H_2 gas) with a minimum concentration of 1.0 ppm. Therefore, it can be concluded that the present CuO/Fe_3O_4 based sensors are selective toward H_2S gas. Furthermore, pristine CuO nanoparticles were tested for their sensitivity against H_2S in a separate study, and they were sensitive for a minimum concentration of 10 ppm [14], while pristine Fe_3O_4 nanoparticles are tested for their sensitivity for H_2S in this work and they do not exhibit any response. Accordingly, the present sensors based on CuO/Fe_3O_4 nanoparticles exhibit enhanced sensitivity as compared with either of the pristine CuO and Fe_3O_4 based sensors. The effect of humidity on the sensor is examined. Herein, the sensor is placed in the lab under normal humidity of 30% for 24 h, and then tested for its response. The sensor is placed in the test chamber under the flow of gas mixture with zero

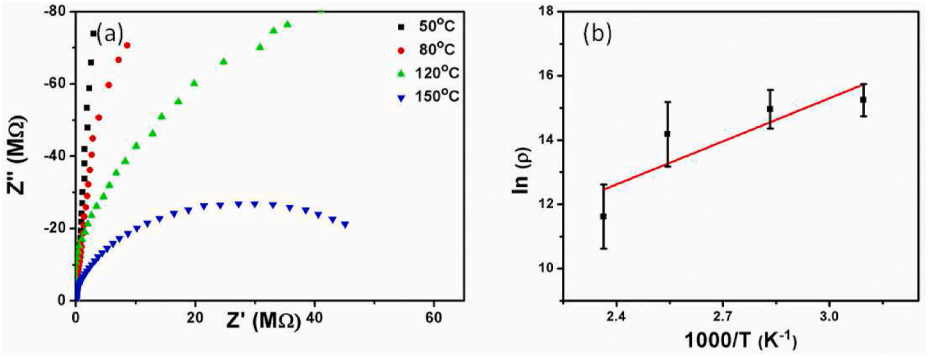

Fig. 3. *(a) Nyquist plot for* CuO/Fe_3O_4 *nanoparticles at different temperatures as a function of frequency as an implicit variable. (b) The invers temperature dependence of the resistivity on natural logarithmic scale for* CuO/Fe_3O_4 *nanoparticles.*

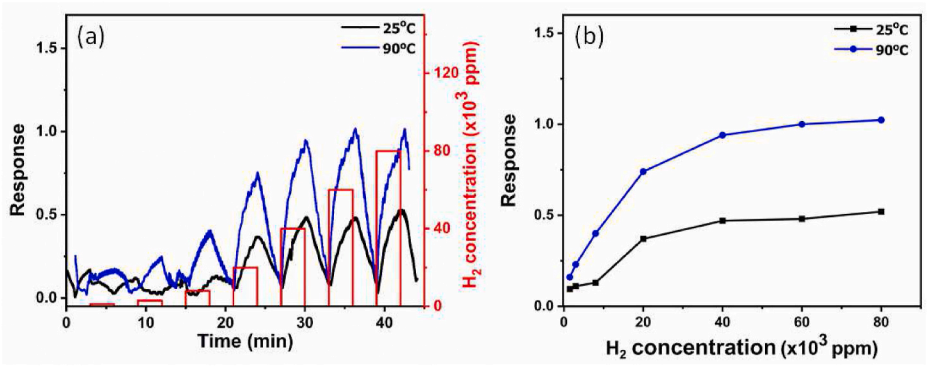

Fig. 4. *(a) Signal, (b) response, and (c) response time of the sensor based on* CuO/Fe_3O_4 *nanoparticles towards* H_2 *gas at variable gas concentration and different temperatures.*

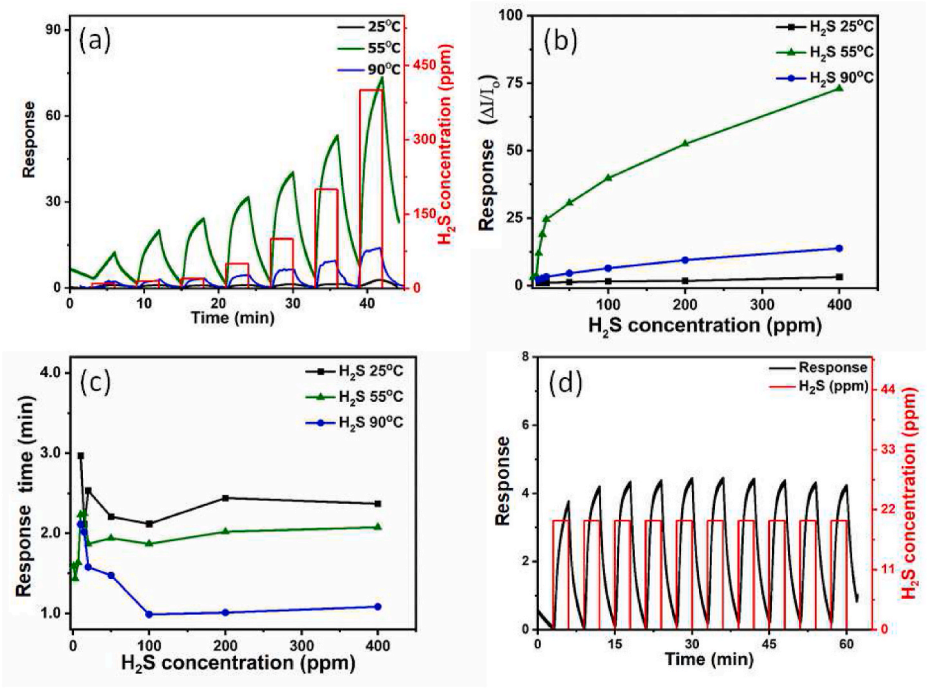

Fig. 5. *(a) Signal, (b) response, and (c) response time of the sensor based on* CuO/Fe_3O_4 *nanoparticles towards* H_2S *gas at variable gas concentration and different temperatures. (d) Sensor stability test at 35 ° C for* 20 ppm *of* H_2S*. The signal of gas sensing at 25 ° C and low* H_2S *concentrations is shown in the supplementary material – S2.*

humidity. The flow of gas inside the test chamber decreases its humidity (surrounding the sensor) gradually during the response test to ~0. Thus, a drift in electrical current to higher values is observed (Supplementary material – S1). Nevertheless, the shape of the signal as well as the current difference (i.e. response) remain the same. Furthermore, the stability of the sensors toward H_2S is measured for 10 cycles for 20 ppm at 35 °C as shown in Fig. 5(d). The device is stale after the second cycle for around 1 h. The devices are tested repeatedly for few days after fabrication, and similar results are obtained. Table 1 presents recent results of sensitivity for sensors based on p-n junctions that include CuO nanoparticles against H_2S gas. The table illustrate great enhancement of the sensitivity for the present sensor.

In general, nanoparticles are more effective for gas sensor applications, as associated with their bulk equivalents, because of their high surface area as compared with volume. The enhanced response of the present sensors toward H_2S in particular may be allocated to the adsorption of oxygen spices (such as O^- as well as O^{2-}) on n the surface of nanoparticles' reactive sites during exposure to H_2S which raise the concentration of charge carriers and hence gas response [30]. Free electrons are generated due to adsorption of oxygen ions on the reactive cites of CuO/Fe_3O_4 because of exposure to H_2S gas, and they are driven due to the applied electric field. The adsorption process of oxygen ions

Table 1
Reported sensitivity results against H_2S *gas for sensors based on p-n junctions and include CuO nanoparticles.*

p-n junction material	Minimum H_2S concentration (ppm)	Operation temperature (°C)	Reference
NiO/CuO nanotubular	5.0	50	[26]
CuxO:SnO_2 nanorod	5.0	24	[27]
ZnO/CuO composites	10.0	40	[28]
ZnO@CuO hollow spheres	10.0	25	[9]
ZnO/CuO thin film	5.0	250	[29]
CuO/Fe_3O_4 nanoparticles	1.0	25	This work

may be described as [31]:

$$H_2S + 3O^{x-}(ads) \rightarrow H_2O + SO_2 + (3x)e^- \quad (1)$$

where in equation (1) $x = 1$ *or* 2. Therefore, the growth of sensor response is assigned to the production of free electrons that are proportional to the concentration of the adsorbed H_2S gas.

The electronic sensitization of CuO/Fe_3O_4 nanoparticles is assigned to the formation of p-n junctions between both semiconductors: the p-type CuO, and n-type Fe_3O_4 as illustrated schematically in inset of Fig. 6. CuO nanoparticles receive electrons from Fe_3O_4 that generates depletion regions for the p−n junctions on the interfaces that cause increasing the resistance [32]. The depletion regions are stronger than those generated by the adsorbed oxygen on top of Fe_3O_4 nanoparticles, thus, the resistance raises increasing the sensitivity [33]. The higher the temperature, the lower the energy required for the charge carriers to cross the junction. It should be noted that the barrier height at grain boundary is constant for the sensor at constant temperature. The number of released free electrons decreases once the flow of H_2S is paused and the sensor is "washed" with air. Accordingly, the gas sensing function is reversible, and the produced sensors based on CuO/Fe_3O_4 are useable for several examination cycles. The released free electrons might be trapped at the surface of CuO/Fe_3O_4 by defects or depletion regions of the p-n junctions which necessitates extra energy to mobilize them within the network of nanoparticles. Therefore, the electrons are driven by the bias voltage through the junction shown by the inset of Fig. 6. Additionally, increasing the temperature to 55 °C releases trapped electrons due to the increase of their heat energy and produces higher response. Nevertheless, further increase of temperature decreases the response which may be assigned to the high percentage of excited charge due to heat energy rather than adsorption of H_2S gas.

The above mechanism is supported by I(V) measurements of the sensor before and after exposure to H_2S gas as depicted in Fig. 6. The figure demonstrates that almost linear I(V) characteristic which is expected at low voltage for granular systems while non-linearity is more clear at high voltages [24]. The figure presents the negative temperature coefficient of the resistance illustrated in Fig. 3. More important, the figure demonstrates higher conductance after exposure to H_2S gas which indicates the presence of excess charges generated due to the adsorption of adsorption of oxygen ions.

Time of response of a sensor is an important factor that determines its usability as a commercial H_2S field sensor, and it is described as the time duration for response to record 90% of its highest value. The response times at different temperatures of the present sensors based on CuO/Fe_3O_4 for H_2S are illustrated in Fig. 5(c). The figure presents that the average sensor response time towards H_2S span between 1.0 and 2.5 min. Furthermore, the response time is almost constant at a fixed temperature for different H_2S concentrations (higher than 50 ppm), and it decreases with increasing temperature. The reduction of response time with increasing temperature is due to the gained kinetic energy of the charge carriers that reduces the time they need to reach to the sensor electrodes. The low values of response time at low temperatures ($\leq$ 90 °*C*) are considered substantial enhancement of the H_2S sensor systems [34–36].

4. Conclusion

Fe_3O_4 nanoparticles decorated with CuO were synthesized in this work and investigated for their application to fabricate H_2S gas sensor applications. The nanoparticles were synthesized by a coprecipitation method with average sizes of 33.33 ∓ 5.55 *nm* and 9.72 ∓ 1.39 *nm* for Fe_3O_4 and CuO, respectively. The nanoparticles were deposited on printed substrates with pre-formed interdigitated electrodes to fabricate the sensor devices. Impedance spectroscopy tests illustrated the semiconductor performance of the nanoparticles with an activation energy of 0.386 ± 0.076 *eV*. The sensors fabricated her were selective towards H_2S, exceedingly sensitive at low temperature with a response of 1.0 ppm, and exhibit low response time with a minimum of 1.0 min. The implementation of magnetic nanoparticles within the fabricated sensors promotes material recycling for additional application rounds. The fabricated H_2S sensors have many attractive features including simplified practical fabrication process, low power need, high response, and short response time.

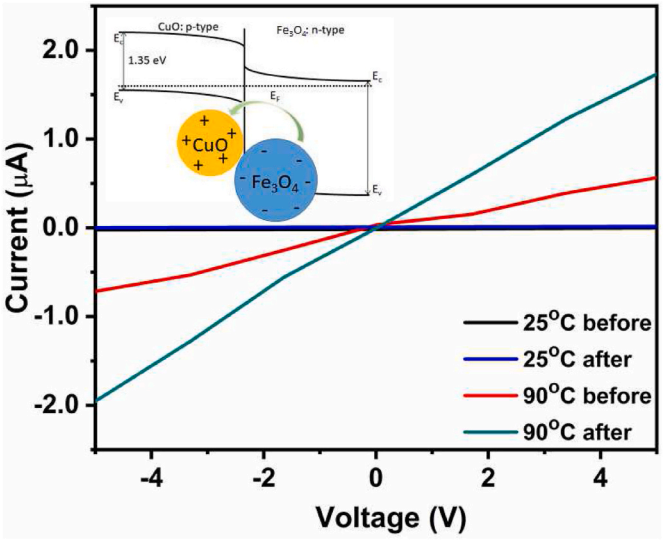

Fig. 6. *I(V) characteristics of the produced sensor based on* CuO/Fe_3O_4 *nanoparticles at different temperatures before and after exposure to* H_2S *gas. The inset is a schematic diagram of the p-n junction.*

Data availability

The raw data required to reproduce these findings are available on request from the author.

CRediT authorship contribution statement

Ahmad I. Ayesh: Conceptualization, Methodology, Formal analysis, Funding acquisition, Supervision, Writing – original draft, preparation, Writing – review & editing, Project administration, Resources. **Belal Salah:** Investigation, Methodology, Data curation.

Declaration of competing interest

The authors declare that they have no known competing financial interests or personal relationships that could have appeared to influence the work reported in this paper.

Acknowledgment

This work was supported by Qatar University under grant number, IRCC-2019-003. The XRD, TEM, SEM, and EDS measurements were accomplished in the Central Laboratories unit at Qatar University.

Appendix A. Supplementary data

Supplementary data to this article can be found online at https://doi.org/10.1016/j.matchemphys.2022.125934.

References

[1] F.I. Ali, F. Awwad, Y.E. Greish, S.T. Mahmoud, Hydrogen sulfide (H 2 S) gas sensor: a review, IEEE Sensor. J. 19 (2018) 2394–2407.

[2] W. Jaeschke, H. Claude, J. Herrmann, Sources and sinks of atmospheric H2S, J. Geophys. Res.: Oceans 85 (1980) 5639–5644.
[3] G.A. Poda, Hydrogen sulfide can be handled safely, Arch. Environ. Health 12 (1966) 795–800.
[4] A.I. Ayesh, Metal/metal-oxide nanoclusters for gas sensor applications, J. Nanomater. (2016) 2016.
[5] M. Rosenberg, G. Kulkarni, A. Bosy, C. McCulloch, Reproducibility and sensitivity of oral malodor measurements with a portable sulphide monitor, J. Dent. Res. 70 (1991) 1436–1440.
[6] M. Gaidi, Nanostructured SnO 2 thin films: effects of porosity and catalytic metals on gas-sensing sensitivity, Appl. Phys. A 124 (2018) 1–14.
[7] E. Comini, G. Faglia, G. Sberveglieri, Z. Pan, Z.L. Wang, Stable and highly sensitive gas sensors based on semiconducting oxide nanobelts, Appl. Phys. Lett. 81 (2002) 1869–1871.
[8] G. Chaloeipote, R. Prathumwan, K. Subannajui, A. Wisitsoraat, C. Wongchoosuk, 3D printed CuO semiconducting gas sensor for ammonia detection at room temperature, Mater. Sci. Semicond. Process. 123 (2021) 105546.
[9] H. Wang, Y. Luo, B. Liu, L. Gao, G. Duan, CuO nanoparticle loaded ZnO hierarchical heterostructure to boost H2S sensing with fast recovery, Sensor. Actuator. B Chem. 338 (2021) 129806.
[10] S.H. Joo, D. Zhao, Environmental dynamics of metal oxide nanoparticles in heterogeneous systems: a review, J. Hazard Mater., (https://doi.org/10.1016/j.jhazmat.2016.02.068)..
[11] Y. Wu, N. Huang, J. Wang, Sensitive characteristics of ZnO nano gas sensor based on dynamic temperature modulation, Results Phys. 18 (2020) 103241.
[12] J.-H. Park, K. Natesan, Oxidation of copper and electronic transport in copper oxides, Oxid. Metals 39 (1993) 411–435.
[13] T. Bhowmick, S. Nag, S.B. Majumder, Understanding the ethanol and acetone sensing behaviour of CuO thin films through elements of gas diffusion theory, Mater. Chem. Phys. 262 (2021) 124286.
[14] A.I. Ayesh, A.F.S. Abu-Hani, S.T. Mahmoud, Y. Haik, Selective H2S sensor based on CuO nanoparticles embedded in organic membranes, Sensor. Actuator. B Chem. 231 (2016) 593–600.
[15] T. Nunome, H. Irie, N. Sakamoto, O. Sakurai, K. Shinozaki, H. Suzuki, N. Wakiya, Magnetic and photocatalytic properties of n-and p-type ZnFe2O4 particles synthesized using ultrasonic spray pyrolysis, J. Ceram. Soc. Jpn. 121 (2013) 26–30.
[16] A. Kumar, A. Kumar, G. Sharma, H. Ala'a, M. Naushad, A.A. Ghfar, F.J. Stadler, Quaternary magnetic BiOCl/g-C3N4/Cu2O/Fe3O4 nano-junction for visible light and solar powered degradation of sulfamethoxazole from aqueous environment, Chem. Eng. J. 334 (2018) 462–478.
[17] S. Zhao, Y. Shen, F. Hao, C. Kang, B. Cui, D. Wei, F. Meng, P-n junctions based on CuO-decorated ZnO nanowires for ethanol sensing application, Appl. Surf. Sci. 538 (2021) 148140.
[18] H. Zhao, X. Ning, H. Yao, A. Hao, M. Ismail, Facile sol-gel method derived Au nanoparticles decoration nickel ferrites thin films: effect on optical and magnetic properties, Mater. Chem. Phys. 265 (2021) 124480.
[19] H. Singh, J. Du, P. Singh, G.T. Mavlonov, T.H. Yi, Development of superparamagnetic iron oxide nanoparticles via direct conjugation with ginsenosides and its in-vitro study, J. Photochem. Photobiol. B Biol. 185 (2018) 100–110.
[20] M.A. Haija, A.I. Ayesh, S. Ahmed, M.S. Katsiotis, Selective hydrogen gas sensor using CuFe2O4 nanoparticle based thin film, Appl. Surf. Sci. 369 (2016) 443–447.
[21] E. Solano, C. Frontera, T. Puig, X. Obradors, S. Ricart, J. Ros, Neutron and X-ray diffraction study of ferrite nanocrystals obtained by microwave-assisted growth. A structural comparison with the thermal synthetic route, J. Appl. Crystallogr. 47 (2014) 414–420.
[22] O. Garcia-Martinez, R. Rojas, E. Vila, J.M. De Vidales, Microstructural characterization of nanocrystals of ZnO and CuO obtained from basic salts, Solid State Ionics 63 (1993) 442–449.
[23] L.A. Al-Sulaiti, B. Salah, A.I. Ayesh, Investigation of flexible polymer-Tl2O3 nanocomposites for x-ray detector applications, Appl. Surf. Sci. 489 (2019) 351–357.
[24] A.I. Ayesh, Electronic transport in Pd nanocluster devices, Appl. Phys. Lett. 98 (2011) 133108.
[25] M.A. Haija, A.F.S. Abu-Hani, N. Hamdan, S. Stephen, A.I. Ayesh, Characterization of H2S gas sensor based on CuFe2O4 nanoparticles, J. Alloys Compd. 690 (2017) 461–468.
[26] L. Sui, T. Yu, D. Zhao, X. Cheng, X. Zhang, P. Wang, Y. Xu, S. Gao, H. Zhao, Y. Gao, In situ deposited hierarchical CuO/NiO nanowall arrays film sensor with enhanced gas sensing performance to H2S, J. Hazard Mater. 385 (2020) 121570.
[27] G. Zhu, H. Xu, Y. Xiao, Y. Liu, A. Yuan, X. Shen, Facile fabrication and enhanced sensing properties of hierarchically porous CuO architectures, ACS Appl. Mater. Interfaces 4 (2012) 744–751.
[28] T. Kida, S. Fujiyama, K. Suematsu, M. Yuasa, K. Shimanoe, Pore and particle size control of gas sensing films using SnO2 nanoparticles synthesized by seed-mediated growth: design of highly sensitive gas sensors, J. Phys. Chem. C 117 (2013) 17574–17582.
[29] C. Han, X. Li, C. Shao, X. Li, J. Ma, X. Zhang, Y. Liu, Composition-controllable p-CuO/n-ZnO hollow nanofibers for high-performance H2S detection, Sensor. Actuator. B Chem. 285 (2019) 495–503.
[30] F.-N. Meng, X.-P. Di, H.-W. Dong, Y. Zhang, C.-L. Zhu, C. Li, Y.-J. Chen, Ppb H2S gas sensing characteristics of Cu2O/CuO sub-microspheres at low-temperature, Sensor. Actuator. B Chem. 182 (2013) 197–204.
[31] A.I. Ayesh, A.A. Alyafei, R.S. Anjum, R.M. Mohamed, M.B. Abuharb, B. Salah, M. El-Muraikhi, Production of sensitive gas sensors using CuO/SnO 2 nanoparticles, Appl. Phys. A 125 (2019) 1–8.
[32] F.E. Annanouch, Z. Haddi, S. Vallejos, P. Umek, P. Guttmann, C. Bittencourt, E. Llobet, Aerosol-assisted CVD-grown WO3 nanoneedles decorated with copper oxide nanoparticles for the selective and humidity-resilient detection of H2S, ACS Appl. Mater. Interfaces 7 (2015) 6842–6851.
[33] C. Wang, Y. Zhang, X. Sun, Y. Sun, F. Liu, X. Yan, C. Wang, P. Sun, G. Lu, Preparation of Pd/PdO loaded WO3 microspheres for H2S detection, Sensor. Actuator. B Chem. 321 (2020) 128629.
[34] N.S. Ramgir, C.P. Goyal, P.K. Sharma, U.K. Goutam, S. Bhattacharya, N. Datta, M. Kaur, A.K. Debnath, D.K. Aswal, S.K. Gupta, Selective H2S sensing characteristics of CuO modified WO3 thin films, Sensor. Actuator. B Chem. 188 (2013) 525–532.
[35] J. Liu, X. Huang, G. Ye, W. Liu, Z. Jiao, W. Chao, Z. Zhou, Z. Yu, H2S detection sensing characteristic of CuO/SnO2 sensor, Sensors 3 (2003) 110–118.
[36] Y.-J. Chen, F.-n. Meng, H.-l. Yu, C.-l. Zhu, T.-s. Wang, P. Gao, Q.-y. Ouyang, Sonochemical synthesis and ppb H2S sensing performances of CuO nanobelts, Sensor. Actuator. B Chem. 176 (2013) 15–21.